

SIZE-FREQUENCY DISTRIBUTIONS OF DUST-SIZE DEBRIS FROM THE IMPACT DISRUPTION OF CHONDRITIC METEORITES

Daniel D. Durda⁽¹⁾, George J. Flynn⁽²⁾, L. Erica Sandel⁽³⁾, Melissa M. Strait⁽³⁾

⁽¹⁾Southwest Research Institute, 1050 Walnut Street, Suite 400, Boulder, CO 80302 USA
Email: durda@boulder.swri.edu

⁽²⁾State University of New York Plattsburgh, Plattsburgh, NY 12901 USA

⁽³⁾Alma College, Alma, MI 48801 USA

ABSTRACT/RESUME

We present mass-frequency data for fragments from the impact disruption of four chondritic meteorites, extending to masses several orders of magnitude smaller than the mass-frequency data that are usually measured in similar impact experiments. Masses of mm- to cm-scale fragments were determined by directly weighing debris collected from the floor of the Ames Vertical Gun Range impact chamber. Masses of sub-mm to dust-size fragments were determined from analysis of foil penetration data. The mass-frequency distributions display a range of morphologies ranging from nearly linear power-law distributions to ‘broken’ power laws with progressively shallower slopes at smaller fragment masses, apparently dependent on the magnitude of the impact specific energy.

1. INTRODUCTION

In order to understand the collisional evolution of asteroids and interplanetary dust and to accurately model the infrared signature of small particles in our own Solar System and in other young planetary systems, we must address the fundamental problem of better understanding dust production from primary impact disruption events covering a wide range of sizes. At present, however, we understand well the size-frequency distributions (SFDs) for collision fragments within only a couple orders of magnitude of the size scale of the original target body; for impact disruption events at all size scales we still know next to nothing (and in many cases identically nothing) about the primary production of fragments many orders of magnitude smaller than the original target body size. Thus, existing modeling results in these areas have tremendous uncertainties.

Laboratory-scale impact experiments can provide direct knowledge of the SFDs of dust-size debris produced directly from the impact disruption of ~5-cm scale meteorite targets, roughly the size scale of the immediate parent bodies of zodiacal dust particles.

Here, we report results of a set of impact disruption experiments involving chondritic meteorite samples, conducted at the NASA Ames Vertical Gun Range (AVGR). Preliminary results from some of these experiments were reported previously in [1].

2. IMPACT EXPERIMENTS

Chondrite meteorites were impacted by small aluminum projectiles at speeds of about 5 km/s in order to examine the production of dust particles and the mechanics of fracture of real meteoritic materials under the impact regimes that presently exist in the main asteroid belt. Table 1 summarizes the experiment conditions for the shot data presented here. The ~5 cm-scale targets were each suspended at the center of the AVGR impact chamber and surrounded by (typically) four passive dust ‘detectors’ consisting of thin aluminum foils (~7- and 13- μ m thick, mounted in 35mm slide mounts, and 51- μ m thick, taped across larger cutouts in the detector foam core backing) and rectangular blocks of aerogel (with dimensions of ~2 \times 2 \times 3 cm).

Table 1. Conditions for meteorite impacts

AVGR Shot #	Target Mass (gm)	Mass of Largest Fragment (gm)	Impactor	Impactor Speed (km/s)
011014	235.8	83.312	1/8" Al	4.65
011015	248	1.71	1/4" Al	5.59
011016	106.8	4.955	1/8" Al	4.49
020506	105	11.572	1/8" Al	4.31

Fig. 1 shows one of the detectors in detail and in place in the impact chamber near one of the meteorite targets. The detectors were located ~50 cm from the target meteorite, both ‘uprange’ and ‘downrange’ of the projectile path at azimuths of about 45 degrees to either side of the projectile path. The foils were thin enough to allow high-speed particles to penetrate, providing a size distribution of ejecta; particles captured intact in the aerogel were analyzed *in situ* for chemical composition [2,3]. Impact debris was carefully swept from the impact chamber after each shot; recovery fractions are

typically 98% or more of the original target mass. Fragments larger than ~1mm were weighed in order to produce a mass-frequency distribution for the macroscopic impact debris. The impacts were recorded by 500 fps video.



Figure 1. Passive particle detectors used in AVGR impact experiments to capture and measure the properties of dust-size debris. (Left) Detail showing the arrangement of foils and aerogel in a typical detector layout. ~7-, 13-, and 51- μm thick foils are set along the top, middle, and bottom rows, respectively, with blocks of aerogel set in foam holders between the foils. (Right) Typical deployment of a detector near a meteorite target within the AVGR impact chamber.

3. FOIL HOLE DATA

The techniques for obtaining foil hole diameters are described in detail in [4]. To cover the entire area of a particular foil (equal to the window size of a standard 35mm slide mount), the foil was scanned with a Canon Canoscan FS 4000US slide scanner at 4000 dpi. The resulting 4000×5888 pixel images have a resolution of ~6.3 $\mu\text{m}/\text{pixel}$. Fig. 2 shows an example of a slide foil image scanned previously with a lower resolution, 1350 dpi scanner. Smaller, sample areas of some foils were surveyed with a microscope/video setup at a resolution of ~1.6 $\mu\text{m}/\text{pixel}$.



Figure 2. Slide scanner image of a 7- μm thick foil from detector 3 of AVGR shot 011015 (a 248-gm sample of

Northwest Africa 620, an unclassified ordinary chondrite), which was mounted 48 cm from the target, roughly 240° in azimuth from the direction of the incoming projectile. The image resolution is 1350 dpi.

The holes generally display two distinct morphologies: some appear to represent comparatively low-speed ejecta and tend to lie at the bottom of stretched impact depressions in the foil, while others clearly resulted from high-speed particles, being cleanly punched and displaying surrounding, raised rims.

The hole sizes from the resulting scanner images were determined by analysis with the software package ImageJ from NIH, which was used to determine the area of each hole and to convert that area to the diameter of a circular hole having the same area. The foil hole diameter data were converted to impacting particle diameters using the calibration data of [5], presented in their Fig. 14. We assume here a particle speed of 2 km/s, the slowest of the calibrated impact speeds. To generate a cumulative particle mass-frequency distribution from the foil penetration data in order to combine with and extend the mass-frequency data from larger, weighed fragments, it was then necessary to convert the particle diameter to particle mass. We assume particle densities of 3 gm/cm^3 and 4 gm/cm^3 , roughly bounding the range of densities of silicate minerals in chondritic meteorites. Two sets of data points are shown for the foil data, one for each of the two density assumptions.

4. RESULTS AND DISCUSSION

Analysis of the foil image data is still underway. Results presented here, however, are illustrative of the data sets that are being used to extend the SFDs of the fragments from the disruption of other meteorite samples down to dust-size particles.

The flux of debris ejected from each of the disrupted targets varies significantly in different directions around the target. Most generally, we tend to see a higher flux of debris on the uprange detectors than on the downrange detectors; the difference in uprange and downrange flux can be a factor of a few to several, but in some extreme cases we have observed essentially no holes in the downrange foils. The flux differences vary from shot to shot, though, probably associated with random disruption outcomes dependent in irregular target shape and jetting of debris.

Ideally, each meteorite target would have been completely surrounded by foil, documenting the size frequency distribution of the dust-size fragments over the full 4π geometry. However, this is not practical, since the foil must be rigidly supported to minimize

tearing from low-speed punctures, and it is not practical to count the penetrations in such a large area of foil. So, each of the foils was mounted in a 35mm slide mount, with an exposed area of 8.05 cm². In order to combine the scanner data from the individual foils, the area of each individual foil is normalized to its projected area on a virtual 1-meter radius sphere centered on the target. The ratio of the surface area of the virtual 1-meter radius sphere (125,664 cm²) to the total projected area covered by all the foils for each shot is the correction factor used to scale the foil data particle counts up to full 4 π steradians. These data can now be compared with the mass-frequency distribution of the large fragments that were collected and weighed.

Fig. 3 shows the resulting combined mass-frequency distribution for AVGR shot 020506 (a 105-gm sample of the meteorite Saratov). The foil penetration data (from all eight of the 7- μ m thick foils deployed for this shot) are seen to nicely extend the mass data from the larger collected and weighed fragments (which were weighed to a completeness limit of \sim 0.02 gm). In this and the following figures, the individual data points should be considered to have \sqrt{N} error bars; recall that since the data points for the foil penetration data have been scaled up to 4 π steradians coverage around the target, the error bars here retain their larger, pre-scaled magnitudes.

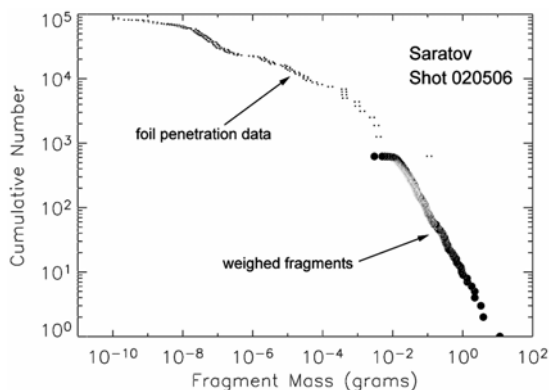


Figure 3. Combined mass-frequency distribution for fragments from AVGR shot 020605 (a 105-gm sample of the meteorite Saratov).

The nearly linear, power law-like mass-frequency distribution (with slope index approximately -0.99) displayed by the larger fragments for this shot extends nearly another two orders of magnitude in particle mass, until breaking to a shallower slope (with slope index approximately -0.22) for masses less than a few 10⁻⁴ gm.

Fig. 4 shows the combined mass-frequency distribution for AVGR shot 011014 (a 235.8-gm sample of the meteorite Northwest Africa 791). Here, penetration

data from the 13- μ m thick foils have been included in addition to data from the 7- μ m thick foils.

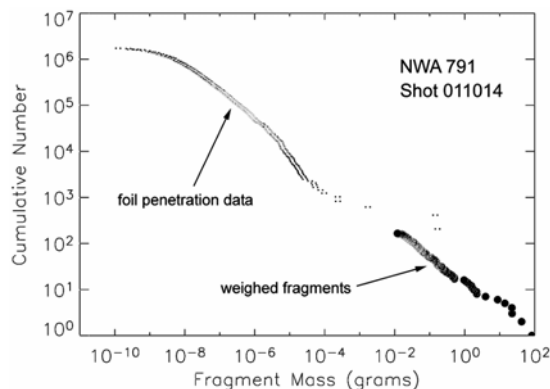


Figure 4. Combined mass-frequency distribution for AVGR shot 011014 (a 235.8-gm sample of the meteorite Northwest Africa 791).

In this case there appears to be a discontinuity in the extension of the weighed fragment data by the foil data. The very largest holes punched through the foils are usually very irregular in outline and their 'torn' morphology strongly suggests that they were formed by low-speed, large particles. In these cases the torn holes can be significantly larger and shaped very differently than the projected area of the particles that formed them. This is evident from inspection of Fig. 2, where the largest hole at the bottom right hand portion of the foil image is clearly non-circular in outline. It is not surprising, then, that the measured areas of the several largest holes may not accurately translate into equivalent particle mass. Thus, the few most massive particles in the foil penetration data may in some cases make seemingly discontinuous extensions of the weighed fragment mass-frequency distributions.

Figs. 5 and 6 show the combined mass-frequency distributions for AVGR shot 011015 (a 248-gm sample of the meteorite Northwest Africa 620) and AVGR shot 011016 (a 106.8-gm sample of the meteorite MOR 001). As in the case for shot 011014, penetration data from both the 7- μ m and 13- μ m thick foils are included, although for shot 011016 scans of only two foils of each size were available from each of two detectors, and those foils were previously scanned at a lower resolution of 1350 dpi.

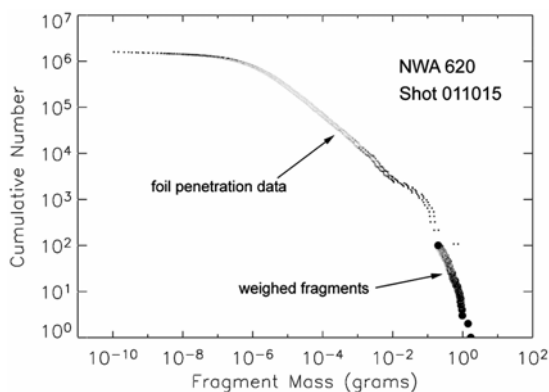


Figure 5. Combined mass-frequency distribution for AVGR shot 011015 (a 248-gm sample of the meteorite Northwest Africa 620).

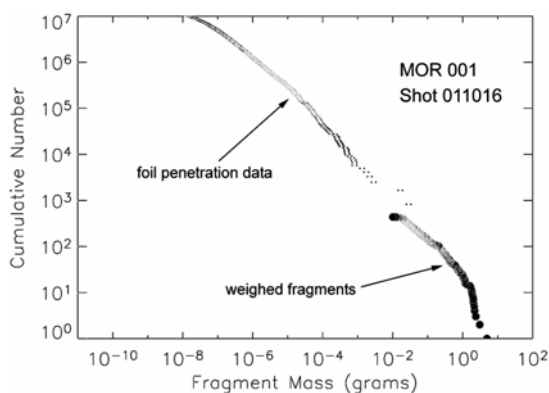


Figure 6. Combined mass-frequency distribution for AVGR shot 011016 (a 106.8-gm sample of the meteorite MOR 001).

The slope indices of the mass-frequency distributions for shots 011014 and 011015 should be compared with respect to the specific impact energies of each shot. In both cases ~ 240 -gm target meteorites were disrupted, but for shot 011014 the impactor was a $\frac{1}{8}$ -in aluminum sphere impacting at 4.65 km/s while for shot 011015 the impactor was a $\frac{1}{4}$ -in aluminum sphere impacting at 5.59 km/s. The specific impact energies for the two shots were approximately 2086 J/kg and 22932 J/kg, respectively. The catastrophic disruption of the target in shot 011014 resulted in an nearly linear mass-frequency slope index of about -0.58, while the supercatastrophic disruption in shot 011015 resulted in a 'broken' mass-frequency distribution (like shot 020506) with slope indices of about -2.22 and -0.65 for the larger and smaller fragments, respectively.

Shot 011016 represents an intermediate case with a specific impact energy of approximately 4294 J/kg. The slope index is approximately -0.83 for fragments with masses less than about 1 gm.

Although we have made the implicit suggestion here that the specific impact energy may be a significant factor in determining the differences in morphology of the mass-frequency distributions from these disruptive impacts, it may well be that simple random variations in shot conditions, target shape, and/or target material properties are at least as important.

Similar data from the foils from 10 other shots conducted to date involving chondritic meteorite targets are being combined to extend the mass frequency distributions of mm- to cm-scale fragments down to dust-size particles. These dust SFDs are providing very useful knowledge of the primary fragment SFDs to much smaller sizes than is conventionally measured in laboratory impact experiments.

5. REFERENCES

- [1] Durda D. D., Flynn G. J., Hart S. D., and Asphaug E. (2002) *LPS*, XXXII, abstract #1535.
- [2] Flynn G. J and Durda D. D. (2004) *Planet. Space Sci.*, **52**, 1129-1140.
- [3] Flynn G. J. et al. (1996) *LPS*, XXVII, 369.
- [4] Sandel L. E., M. M. Strait, D. D. Durda, and G. J. Flynn (2006) *LPS*, XXXVII.
- [5] Hörz F. et al. (1995) *NASA Technical Memorandum 104813*.